Tuning of plasmonic surface lattice resonances: on the crucial impact of the excitation efficiency of grazing diffraction orders

*Lynda Dehbi Kartikey Pandey Macilia Braïk Stéphanie Lau-Truong Abderrahmane Belkhir Sarra Gam-Derrouich Alexandre Chevillot-Biraud Claire Mangeney Abdelaziz Mezeghrane Fadi Issam Baida Nordin Félidj**

Lynda Dehbi, Macilia Braïk, Abdelaziz Mezeghrane, Abderrahmane Belkhir
Université Mouloud Mammeri de Tizi Ouzou, LPCQ, BP 17 RP, 15000 Tizi-Ouzou, Algeria
Claire Mangeney
Université Paris Cité, LCPBT, CNRS, F-75006 Paris, France
Fadi Issam Baida
Université de Bourgogne Franche-Comté, FEMTO-ST, CNRS, 25030 Besançon Cedex, France
Kartikey Pandey, Stéphanie Lau-Truong, Sarra Gam-Derrouich, Alexandre Chevillot-Biraud, Nordin Félidj*
Université Paris Cité, ITODYS, CNRS, F-75006 Paris, France
Email Address*: nordin.felidj@u-paris.fr

Keywords: *plasmonics, surface lattice modes, Rayleigh anomaly, diffraction orders*

Metallic nanoparticles exhibit remarkable optical properties through localized surface plasmon (LSP) resonances. When arranged in arrays, nanoparticles form surface lattice resonances (SLRs) affected by inter-particle distance. SLRs offer narrower bandwidths and stronger electric field enhancements than LSP modes, crucial for efficient optical device development. Efficient grazing diffracted orders crucially impact SLR properties, facilitating long-range nanoparticle interactions. This study explores how photonic modes in the substrate plane influence SLRs using experimental and theoretical approaches, including Finite Difference Time Domain simulations on gold disk arrays. Results show SLR properties strongly rely on diffracted mode efficiency controlled by the grating constant and incident polarization. Notably, large inter-particle spacing and incident polarization can eliminate the grating effect. Understanding and managing long-range interactions in engineered plasmonic structures are highlighted, providing insights for enhanced performance in advanced photonic and optoelectronic devices.

1 Introduction

Metallic nanoparticles (NPs) possess a remarkable ability to absorb or scatter light thanks to their capability to sustain localized surface plasmon (LSP) resonances [1, 2, 3]. These resonances correspond to the coherent oscillations of surface conduction electrons in response to the incident electric field of light, leading to the emergence of an enhanced optical near-field[4, 5, 6]. The increase of the local field strength originates from significant polarization at optical frequencies induced by the electron oscillation. The LSP frequency of a metallic nanoparticle is closely linked to the plasma frequency of the free electrons, a parameter determined by the particle's size and shape, as well as the permittivity of the metal and the surrounding medium [7, 8, 9]. When these nanoparticles are arranged in a periodic lattice, their plasmonic resonances can couple with each other, leading to the emergence of new resonant modes called surface lattice resonances (SLRs)[10, 11]. SLR occurs if the diffraction order of a periodic array becomes a surface wave propagating in the plane of the grating, known as the Rayleigh anomaly (RA)[12, 13]. In other words, SLR originates from the coupling between localized surface plasmon modes and grazing diffraction modes. Their frequency are influenced not only by the optical response of individual nanoparticles but also by the lattice parameters such as the inter-particle distance (grating constant) and the array configuration. They are characterized by a narrow bandwidth implying a strong enhancement of the electric field in the vicinity of the particles[14, 15]. In the far-field, this long-distance coupling is evidenced by a red-shift in the wavelength of SLR mode as the grating constant increases, reaching a maximum of spectral shift for grating constant close to the incident light wavelength. Collective effects in 2D periodic arrays of nanoparticles have been investigated in numerous studies for fundamental understanding of the SLR effect [16, 17], and more recently in order to improve optical responses that are often not possible with single particles, such as high quality factors [18, 19]. Indeed, such long-range interactions

are particularly interesting since it results in improved enhanced light-matter interaction, compared to non-coupled nanoparticles, including enhanced light absorption, scattering, and confinement of electromagnetic fields within the structures array, with distinct applications including sensing [20], enhanced spectroscopy [21, 22], and photonic devices [23]. However, no study has yet examined the impact of the efficiency of diffracted orders in the substrate plane that facilitate coupling between the particles at long distances. This aspect is of crucial importance since it opens up the route for improvements in the monitoring of the long-range interactions, and in particular, of the SLR wavelengths. Therefore, this study addresses the following questions: is there a significant impact of the efficiency of diffracted orders in the plane of the substrate on the SLR properties? And as a possible consequence, can we monitor the SLR properties through the control of the photonic modes propagating in the plane of the substrate?
To raise these questions, we propose in this article, to study experimentally the SLR properties supported by rectangular arrays of gold nanoparticles, elaborated by electron beam lithography [24], and theoretically through Finite Difference Time Domain (FDTD) simulations[25, 26]. Indeed, considering rectangular arrays, will allow us to analyze the efficiency of the diffracted modes by changing the grating constant according to the direction of the incident polarization, and see the impact on the SLR resonance along the perpendicular direction, as schematized in **Figure 1**. In doing this, we will show that the grazing modes propagating perpendicularly to the incident light polarization, at normal incidence, are strongly affected by the grating constant according to the incident polarization, using, as model systems, dielectric NPs. As a strong consequence, it is shown that the grating effect is totally annihilated, for large inter-particle spacing according to the incident polarization. Finally, the rectangular configuration presents a strong added value for precise engineering of plasmonic structures, allowing for tailored optical responses. Understanding and harnessing these resonances offer opportunities for developing advanced photonic and optoelectronic devices with enhanced performance and functionalities.

2 Results and discussion

To date, the majority of fundamental and applied studies on surface lattice resonance (SLR) have focused mainly on square or hexagonal arrays of nanoparticles [11, 27, 28], while others have studied the impact on coupling to the Rayleigh anomaly by modifying the size of the nanoparticles, which can also alter the surface plasmon response [29, 30].
To achieve our goal, we will consider rectangular arrays of gold nano-disks, and show that such configuration enables us to elucidate the pivotal role of diffracted modes in SLR properties. Only a limited number of papers have addressed the utilization of rectangular arrays made of metallic nano-disks, primarily within the context of Surface-Enhanced Raman Spectroscopy (SERS) experiments[31]. The distinct rectangular arrays of gold nano-disks are fabricated via Electron Beam Lithography (EBL), featuring a diameter (D) of 150 nm and a fixed height (h) of 50 nm. The grating constants in the x- and y-directions are denoted as P_x and P_y, respectively. The gold nano-disks are deposited onto a glass substrate coated with a thin layer of Indium Tin Oxide (ITO) measuring 80 nm in thickness. The structure is illuminated by a linearly polarized plane wave along the x-axis from the substrate side. This polarization direction enables the excitation of Rayleigh anomalies propagating along the y-direction. The transmitted signal is collected in the same direction in air, and it is processed to determine the extinction spectra. The investigation into the impact of the distance between nanoparticles along the polarization axis on the position of SLR resonances is then made possible by simply varying P_x, as depicted in Figure 1.
To explore the influence of the grating constant aligned with the polarization direction of the incident light (e.g., along the x-axis) on the position of the SLR, we initially examined two arrays, with identical nanoparticle (diameter $D = 150$nm) and a fixed y-axis period ($P_y = 450$nm), while possessing two distinct x-axis periods ($P_x = 220$nm and $P_x = 400$ nm). The fixed value of P_y at 450nm is chosen strategically to align the spectral position of the RAs$(0, \pm 1)$ closer to that of the LSP resonance of the NPs, thereby entering the regime of long-range interaction (or grating effect). Indeed, the slight disparity between the LSPR and the Rayleigh anomalies $(0, \pm 1)$ enhances the radiative coupling of LSP to grazing

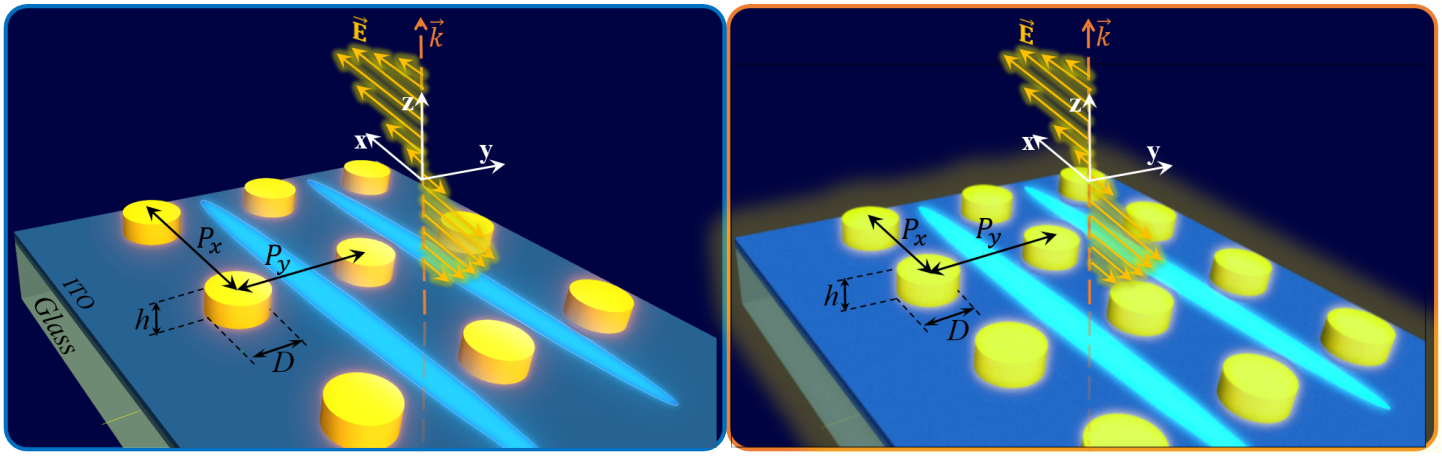

Figure 1: Low diffraction efficiency (in blue box) vs. high diffraction efficiency (in red box) on the surface of rectangular arrays of gold nano-disks featuring a diameter (D) and a fixed height (h). The grating constants in the x- and y-directions are denoted as P_x and P_y, respectively. The gold nano-disks are deposited onto a glass substrate coated with a thin layer of ITO. The polarization set along x-direction enables the excitation of Rayleigh anomalies propagating along the y-direction. The grating effect on SLRs is more important when the diffraction efficiency of the grazing orders is high, i.e. more energy is channeled onto the surface, which is obtained for small interparticle distances along the polarization direction.

diffracted orders. The experimental and FDTD extinction spectra of the two arrays are recorded with a polarization along the x axis, and presented in **Figure 2**. Thus, polarization along the x-axis induces a diffracted mode perpendicular to it, namely, along the y-axis. The spectra show that the RAs$(0, \pm 1)$ interact with the LSPR of the NPs, giving rise to an SLR mode, as anticipated. However, the experimental spectra, in close agreement with FDTD simulations, evidence a higher unexpected red-shift in the position of the SLR for $P_x = 220$nm, compared to that of $P_x = 400$nm. This discrepancy is surprising given that the grating constant along the y-axis ($P_y = 450$nm) remains identical for both arrays.

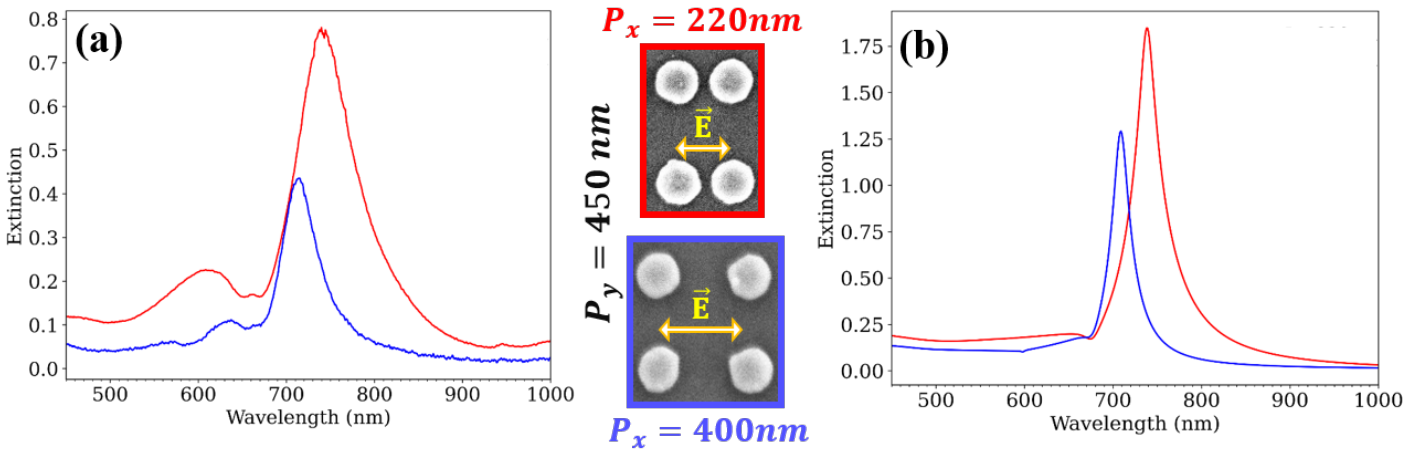

Figure 2: The middle images are SEM images of two rectangular arrays of gold nano-disks with diameter D=150nm, height h = 50nm and y-pitch P_y= 450nm deposited on a glass substrate coated by a thin ITO layer. The image in the red frame corresponds to P_y = 220nm, while the one in the blue frame corresponds to P_y = 400nm. The curves in (a) are the experimental and in (b) the calculated extinction spectra of the structures shown, recorded in the air superstrate when the structure is illuminated at normal incidence from the glass substrate with an x-polarized plane wave. The red curves correspond to $P_x = 220$nm while the blue ones correspond to $P_x = 400$nm.

To confirm the observation, we recorded extinction spectra by varying the grating constants along y-direction, for distinct values of P_x with a polarization along the x-direction, varying from 220nm to 600nm : (a, a') P_x = 220 nm; (b, b') P_x = 300 nm; (c, c') P_x = 400 nm and (d, d') P_x = 600 nm, as shown in **Figure SI1** and **SI2**. We then extracted the experimental and calculated extinction diagrams (see

Figure 3). In all presented cases, the FDTD calculations confirme and closely match the experimental results. Therefore, for identical values of P_y, the resonance wavelength — corresponding to the peak of extinction — is more red-shifted, as P_x decreases. Furthermore, the slope of the resonance band, in the extinction diagram, increases and is red-shifted when P_y increases (prior to reaching strong long-range interaction). This shift becomes particularly significant for small values of P_x. On the contrary, for very large P_x values (for instance $P_x = 600$nm as in Figure 3-(d, d')), the extinction band is almost flat indicating a very weak coupling regime between the RA and the LSP. Same conclusions are observed by considering the similar lattice parameters, but for smaller NPs, with a diameter of $D = 100$nm, as shown in **Figure SI3** and **SI4**. Consequently, the grating constant in the direction of polarization exerts a substantial effect on the SLR spectral position even if the latter is linked to an anomaly propagating in the perpendicular direction (here y-direction).

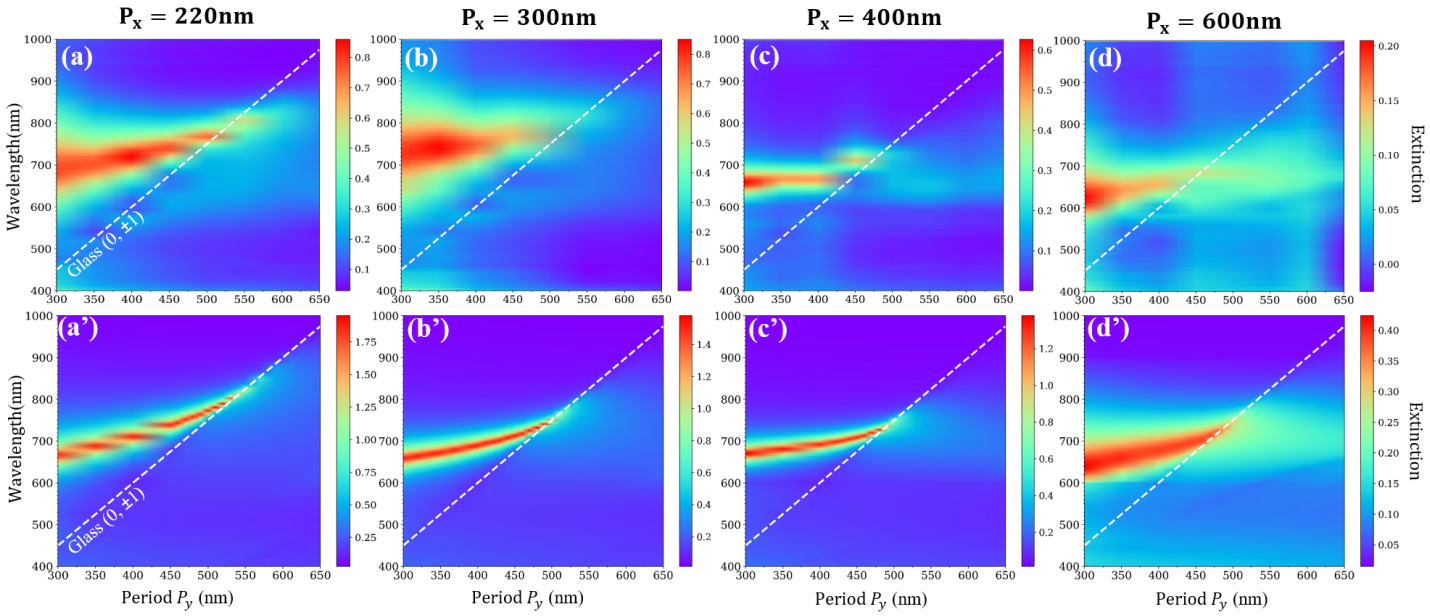

Figure 3: (a-d) Experimental and (a'-d') calculated extinction diagrams of the rectangular arrays of gold nano-disks (150nm in diameter and 50nm high), supported by a glass substrate, for fixed P_x= 220 nm, 300 nm, 400 nm and 600 nm, in this order. The polarization direction of the normal incidence wave is along the x-axis. The Rayleigh anomaly position is displayed in a white line for the $(0, \pm 1)$ orders in the substrate.

In order to elucidate the role of the periodicity in the direction of polarization (here x-direction), the only credible hypothesis is to attribute it to the excitation efficiency (amplitude of the associated electromagnetic field) of the surface wave that is the Rayleigh Anomaly that couples with the LSP giving rise to SLR. To verify this hypothesis, while avoiding absorption phenomena that could influence the amplitudes of the various diffracted modes, we propose to consider a purely dielectric structure. In fact, it is well-known that dielectric nanoparticle arrays could support SLRs resulting from the coupling between Mie resonances of individual particle with the Rayleigh anomaly [32, 33, 34, 35, 36, 37]. Nonetheless, to make sure, we study a grating composed of a rectangular arrangement of dielectric nano-disks made of material with a large refractive index ($n = 4$)[38, 37] of diameter $D = 120$nm and thickness $h = 50$ nm, deposited on a glass substrate. These parameters were chosen so that the scattering efficiency of such an isolated nano-disk (on substrate) exhibits Mie resonance in the visible range as shown in **Figure 4-a**. This resonance is of the electric dipolar type, as can be seen from the distribution of the normalized electric field intensity shown in the inset of Figure 4-a. When we move on to the periodic structure, we set the period along the y-direction to be $P_y = 300$ nm (period perpendicular to the incident polarisation) in order to have RAs $(0, \pm 1)$ in the vicinity of the isolated particle Mie resonance and then, to couple them together to create the SLR. As expected, the extinction spectra of Figure 4-b, obtained for different values of the P_x period show the excitation of such SLRs. As in the case of gold nano-disks grating, these resonances are red-shifted compared to the case of the isolated particle, and

this shift is more important when P_x decreases. Let's now try to determine the very origin of this phenomenon through our above-mentioned assumption involving the modification of the RA's magnitude (efficiency) in the y-direction when the period along the x-direction (P_x) varies. To this purpose, it is necessary to quantify this magnitude as a function of P_x. This requires a configuration where the RAs are far from any interaction with the eigenmodes of the scatterers. The all-dielectric grating offers us this possibility, since the Mie resonance is strongly influenced by the dielectric index of the nanoparticle [38]. An optical refractive index of $n = 2.2$ for the nano-disk shifts the Mie resonance at around 200 nm (see inset in **Figure 5-a**), far from the $(0, \pm 1)$, RA's wavelength which is $450nm$ when P_y is fixed at 300 nm.

Figure 5-a shows the square modulus of the normalized electric field amplitude ($\tau_d = |E_d/E_{inc}|^2$) of the whole diffracted orders by the grating for different values of P_x. This quantity (τ_d) is calculated using relation: $\tau_d = 1 - T_0 - R_0$, where T_0 and R_0 are the specular transmission and reflection coefficients of the structure, respectively. This formula is justified by the inherent non-dissipative nature of our all-dielectric structure, meaning that no energy is lost by absorption. In the case where only the RAs $(0, \pm 1)$ are excited (no more diffracted orders), this electric intensity corresponds to the one carried by these grazing modes. As can be seen in Figure 5-a, the plotted spectra giving the values τ_d for different values of P_x show maxima around $\lambda = 450$ nm whatever the value of P_x. This value corresponds to the energy fraction carried by the diffracted order just before it changes from homogeneous (propagative) to evanescent at $\lambda_{RA} = 450$ nm. This wavelength value is obtained in the case of normal incidence from the formula bellow [39] :

$$\lambda_{RA}(l, m) = n \left[\frac{l^2}{P_x^2} + \frac{m^2}{P_y^2} \right]^{-1/2} \tag{1}$$

Here l and m are the diffracted wave orders along the x and y directions, respectively and n is the optical index of the substrate. Above $\lambda_{RA}(0, \pm 1)$, τ_d decrease rapidly to zero for all values of P_x as seen on Figure 5-a. In this particular spectral range, only evanescent waves are excited as predicted by the formula 1, but without carrying any energy. From these results, we can conclude that this energy fraction associated with the RA$(0, \pm 1)$ is greater when P_x is smaller, i.e. when the nano-disks come closer together along the incident light polarisation direction. The excitation efficiency of these grazing orders is therefore greater the smaller P_x which exalts their coupling with the Mie resonance (or LSP in the case of glod nano-disks).

These observations are corroborated by a band structure calculation carried out on the same structure when the value of P_x is fixed at 250nm (see Figure 5-b). As can be seen in this Figure, the two lower and upper branches are surimposed on the $(0, +1)$ and $(0, -1)$ anomalies; shown as dashed and solid white lines respectively. At the Γ point they tend to the same spectral position (450nm) as that corresponding to the excitation of the two grazing orders $(0, \pm 1)$ by a plane wave illuminating the structure at normal incidence (Figure 5-a). The spectral position of the maximum diffracted energy, independent of P_x and located at the same position as that of the anomalies, indicates the absence of any coupling with the Mie resonances of the nanoparticle (Figure 5-a). This is also confirmed by the absence of additional branches on the band diagram (Figure 5-b).

In a second step, we used the previous dielectric lattice to study the interaction between the Mie resonance and the Rayleigh anomalies by considering the nano-disk index $n = 4$. It is known that a sharp contrast index of the photonic crystal induces the removal of degeneracy at the Γ point, resulting in the appearance of a photonic band gap.

The band calculations carried out on this structure and shown in **Figure 6-a** and **6-b** indicate the presence of 03 branches for the two values of P_x considered. The lower and upper branches are tangent to the $(0, +1)$ and $(0, -1)$ anomalies, shown as dashed and solid white lines respectively. The third central branch corresponds to the localized Mie mode supported by the nano-disks. Near the Γ point, where the coupling is strong, the two band diagrams show only two branches. In this zone, the Mie mode couples with the anomalies, giving rise to two SLRs whose spectral positions are redshifted with respect to the anomaly wavelength. Similar results in relation to plasmonic SLRs were also reported by Tretnak, *et al.*

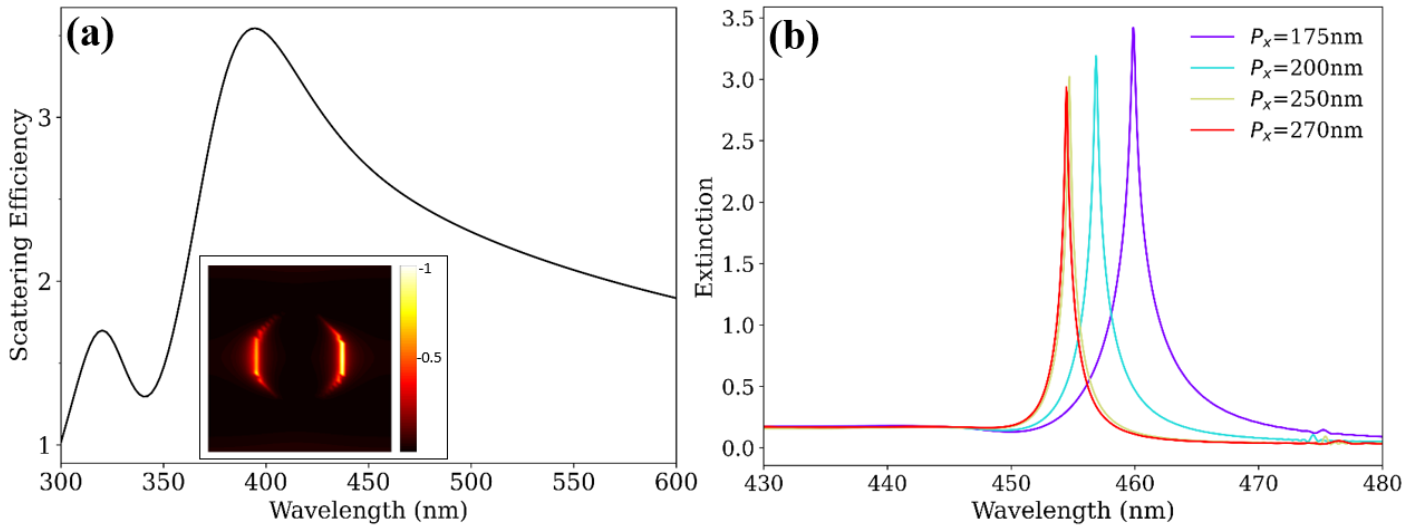

Figure 4: Scattering efficiency of a single dielectric nano-disk of index $n = 4$ in (a), and extinction spectra of dielectric nano-disks' arrays of index $n = 4$ in (b). The inset in (a) corresponds to the electrical intensity distribution in the x-y plane, calculated just below the nano-disk, highlighting the electrically dipolar nature of the Mie resonance. The geometrical parameters of nano-disks are $D = 120$nm as diameter and $h = 50$nm as hight. The lattice parameter P_y is kept constant at 300 nm. Both the single nano-disk and the grating are supported by a glass substrate coated with a thin layer of ITO and surrounded by air as superstrate.

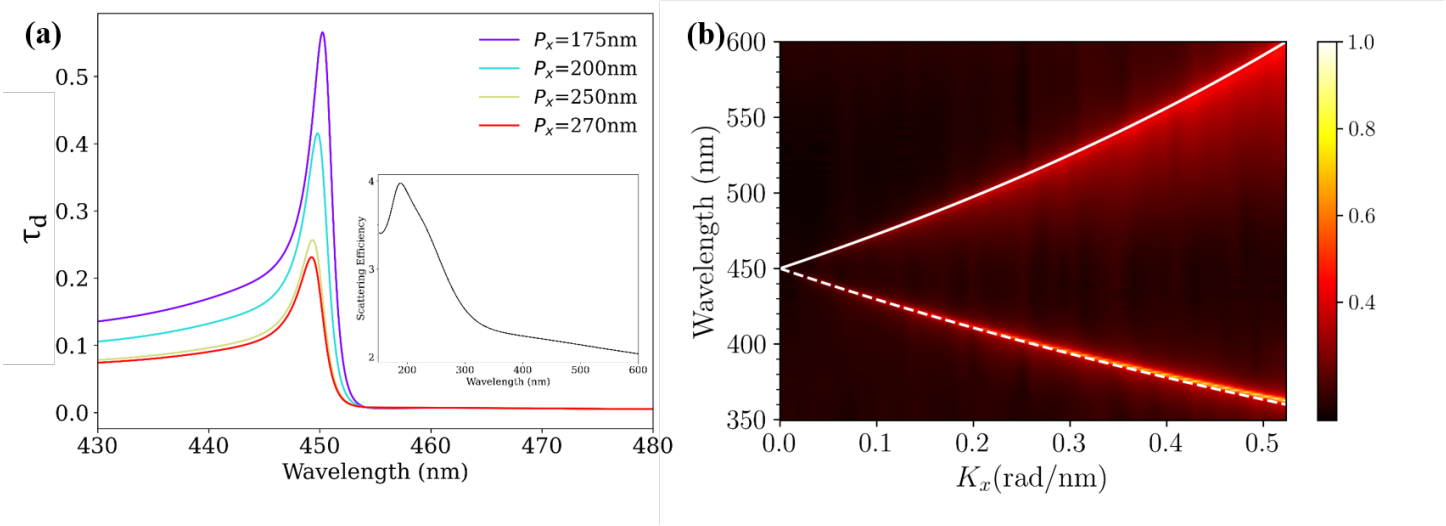

Figure 5: (a) Square modulus of the normalized electric field amplitude spectra of dielectric nano-disks' arrays of index $n = 2.2$ and fixed grating constant $P_y = 300$ nm. The inset corresponds to the scattering efficiency of an isolated nano-disk of index $n = 2.2$.(b) The corresponding Photonic band structure calculated by N-order FDTD for $P_x = 250$nm.The solid and dashed white lines representing the RAs $(0, -1)$ and $(0, +1)$ respectively.

[40].

Outside the strong coupling zone (i.e. far from the Γ point) the three branches coexist. As we move away from the Γ point, the Mie branch tends to flatten out (more rapidly for large P_x), while the other two merge completely with the lattice anomalies. It is important to note that the angular extension (along K_x) of the strong coupling zone is larger the smaller P_x is. In addition, the redshift of the two SLRs near the Γ point is more pronounced when P_x is small. Figure 6-c shows the spectral energy density corresponding to a cross section at the Γ point of the band diagrams in Figure 6-a and 6-b. As can be seen, the redshift is greater for smaller P_x. When compared with the far-field extinction spectra (see Figure 4), it can be seen that the upper branch is a dark mode (absent in the extinction spectra), while the

lower branch is a bright mode (present in the extinction spectra at the same wavelength).

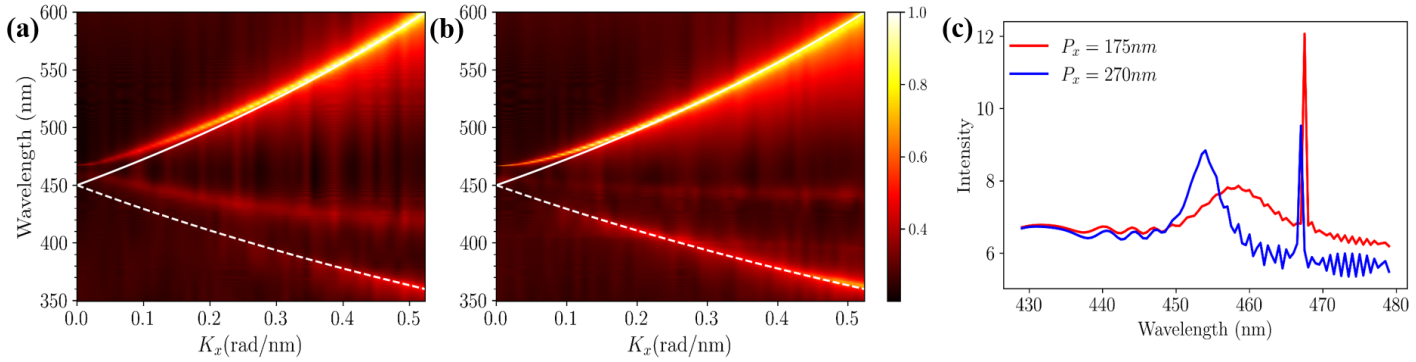

Figure 6: Photonic band structure calculated by N-order FDTD for the dielectric structure of grating constants P_y fixed at $300nm$ and $P_x = 175nm$ in (a) and $P_x = 270nm$ in (b).The solid and dashed white lines representing the RA$(0,-1)$ and RA$(0,+1)$, respectively. (c) Eigenmode calculation at Γ point $(k = 0)$

In **Figure 7** we have superimposed the diffracted energies and the extinctions calculated in the far field in the cases corresponding to the absence ($n = 2.2$, Figure 7-a) and the presence ($n = 4$; Figure 7-b) of the coupling. As can be seen in Figure 7-a, the lack of energy transmitted in the far field, which results in an extinction maximum, is carried on the surface by the grazing orders $(0, \pm 1)$, as confirmed by the superposition of the maxima of the extinction and diffracted energy spectra at wavelength $450nm$. For a scatterers index of $n = 4$, the energy diffracted at the surface is almost zero at about $450nm$, as shown by the red curve in Figure 7-b. This is due to the radiative coupling of the grazing modes with the Mie resonance giving rise to a collective mode (SLR) (in blue in figure 7-b). It can be concluded that for tuning the wavelengths of the grating resonances, the P_x parameter, which is often neglected when the gratings are illuminated by an x-polarised wave, is as important as the P_y parameter. The effect of P_x on the SLR positions is due to the in-plane diffraction efficiency of the $(0, \pm 1)$ orders, which is more important when P_x is small. The spectral position of the SLR is therefore roughly tuned by the pitch along the propagation direction of the anomaly P_y (placing the anomalies close to the single particle resonance) and finely tuned by the pitch along the polarisation direction P_x.

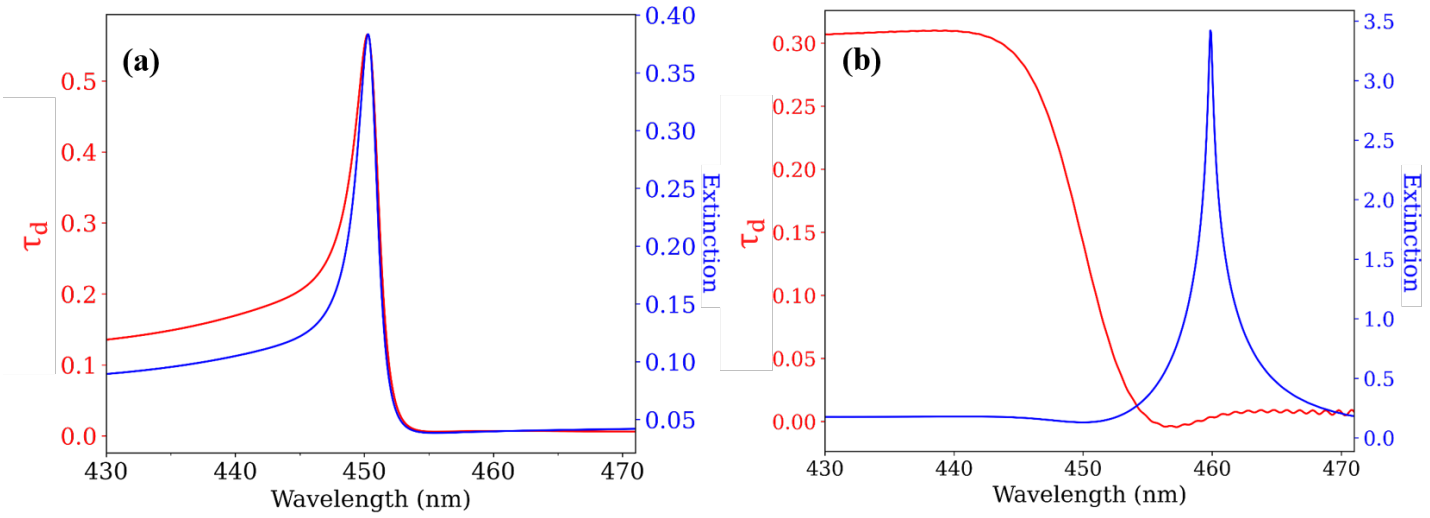

Figure 7: Square modulus of the normalized electric field amplitude and extinction spectra of dielectric nano-disks' arrays vs light wave length when the refractive index of the nano-disk is set equal to $2,2$ in (a) and to 4 in (b). The other parameters are diameter $D = 120nm$, height $h = 50nm$ and periods $P_y = 300nm$ and $P_x = 175nm$. The substrate is glass of index $n = 1.5$

3 Conclusion

In this study, we experimentally investigated SLR properties in rectangular arrays of gold disk particles and complement our findings with Finite Difference Time Domain (FDTD) simulations. By varying the grating constant according to the incident polarization direction, we analyze the efficiency of diffracted modes and their impact on SLR resonance. Our results reveal a strong dependence of SLR properties on the grating constant and incident polarization direction, with the annihilation of the grating effect for large inter-particle spacings. Overall, understanding and manipulating these resonances offer opportunities for developing advanced photonic and optoelectronic devices with enhanced performance and functionalities, underscoring the significance of our findings in advancing nanophotonic engineering.

4 Methods

4.1 Electron beam lithography

The substrates were fabricated by electron beam lithography on modified JEOL scanning electronic microscope (SEM)[24]. A 100nm thick layer of PMMA (poly-methyl methacrylate) electron resist was spin coated on glass substrates covered with a 80nm layer of transparent conducting indium tin oxide (ITO). In the exposure step, the desired structures were exposed to an electron beam which was scanned over the sample. Chemical development, thermal vacuum coating with gold and a lift-off procedure followed, which led to regular arrays of gold nano-disks of the desired cross-section and widths, 50 ± 5 nm height and 100 μm diameter on top of the ITO covered glass-substrate. This method allows us to control precisely the nanoparticle size, shape, and interparticle distance between nanoparticles. We have thus the ability to tune the plasmon resonance at any desired wavelength[24, 41].

4.2 UV-visible extinction spectroscopy

The LSP resonance of the samples were probed by far–field visible-NIR extinction micro-spectroscopy in the range of 500-900 nm, with an irradiation by a halogen lamp from the glass side at normal incidence. The spectrometer (LOT ORIEL model MS 260i) was coupled to an optical microscope (OLYMPUS BX 51) equipped with a 10× objective (numerical aperture N.A. 0.25). The investigated area is a circle of approximately 80 μm diameter, which is smaller than the structures array (100×100 μm^2).

4.3 Finite Difference Time Domain (FDTD) calculations

Finite Difference Time Domain (FDTD) simulations were performed using a developed 3D-code for the optical proprieties investigation. The code takes into account the periodicity of the structure in x and y directions via Bloch's boundary conditions [26] and the upper and lower semi-infinite media in z direction through Perfectly Matched Layers (PML) conditions of Berenger.[42] The implemented Critical Points Drude model [43] deals with the dispersive nature of gold and ITO using different fitted parameters to match experimental values. The structure is illuminated, with a plane wave, at normal incidence from the substrate. In near field, the normalised electric field intensity is calculated in the vicinity of the gold disks, while the detector is placed far away from them for far field simulations of extinction spectra.

Supporting Information
Supporting Information is available from the Wiley Online Library.

References

References

[1] K. M. Mayer, J. H. Hafner, *Chemical reviews* **2011**, *111*, 6 3828.

[2] K. A. Willets, R. P. Van Duyne, *Annu. Rev. Phys. Chem.* **2007**, *58* 267.

[3] Y. Chen, H. Ming, *Photonic Sensors* **2012**, *2* 37.

[4] C. Girard, A. Dereux, *Reports on Progress in Physics* **1996**, *59*, 5 657.

[5] D. W. Pohl, D. Courjon, *Near field optics*, volume 242, Springer Science & Business Media, **2012**.

[6] A. G. Nikitin, A. V. Kabashin, H. Dallaporta, *Optics express* **2012**, *20*, 25 27941.

[7] K. L. Kelly, E. Coronado, L. L. Zhao, G. C. Schatz, The optical properties of metal nanoparticles: the influence of size, shape, and dielectric environment, **2003**.

[8] T. R. Jensen, M. L. Duval, K. L. Kelly, A. A. Lazarides, G. C. Schatz, R. P. Van Duyne, *The Journal of Physical Chemistry B* **1999**, *103* 9846.

[9] M. M. Miller, A. A. Lazarides, *The Journal of Physical Chemistry B* **2005**, *109*, 46 21556.

[10] V. Giannini, G. Vecchi, J. G. Rivas, *Physical review letters* **2010**, *105*, 26 266801.

[11] A. D. Humphrey, W. L. Barnes, *Physical Review B* **2014**, *90*, 7 075404.

[12] D. Maystre, In *Plasmonics: from basics to advanced topics*, 39–83. Springer, **2012**.

[13] A. Maradudin, I. Simonsen, J. Polanco, R. Fitzgerald, *Journal of Optics* **2016**, *18*, 2 024004.

[14] I. Ragheb, M. Braik, A. Mezeghrane, L. Boubekeur-Lecaque, A. Belkhir, N. Felidj, *J. Opt. Soc. Am. B* **2019**, *36*, 7 E36.

[15] L. Zundel, A. May, A. Manjavacas, *ACS Photonics* **2021**, *8*, 1 360.

[16] D. Dey, G. C. Schatz, *MRS Bulletin* **2024**, 1–10.

[17] V. G. Kravets, A. V. Kabashin, W. L. Barnes, A. N. Grigorenko, *Chemical reviews* **2018**, *118*, 12 5912.

[18] K. Yang, Y. Chen, S. Yan, W. Yang, *Heliyon* **2023**.

[19] B. Wang, P. Yu, W. Wang, X. Zhang, H.-C. Kuo, H. Xu, Z. M. Wang, *Advanced Optical Materials* **2021**, *9*, 7 2001520.

[20] Z. Li, C. S. Prasad, X. Wang, D. Zhang, R. Lach, G. V. Naik, *Nanophotonics* **2023**, *12*, 19 3721.

[21] M. Charconnet, C. Kuttner, J. Plou, J. L. García-Pomar, A. Mihi, L. M. Liz-Marzán, A. Seifert, *Small Methods* **2021**, *5*, 10 2100453.

[22] I. Ragheb, M. Braïk, S. Lau-Truong, A. Belkhir, A. Rumyantseva, S. Kostcheev, P.-M. Adam, A. Chevillot-Biraud, G. Lévi, J. Aubard, L. Boubekeur-Lecaque, N. Félidj, *Nanomaterials* **2020**, *10*, 11.

[23] G. Barbillon, *International Journal of Molecular Sciences* **2022**, *23*, 18 10592.

[24] W. Gotschy, K. Vonmetz, A. Leitner, F. Aussenegg, *Applied Physics B* **1996**, *63* 381.

[25] D. M. Sullivan, *Electromagnetic simulation using the FDTD method*, John Wiley & Sons, **2013**.

[26] F. I. Baida, A. Belkhir, Finite difference time domain method for grating structures, **2012**.

[27] R. Guo, T. K. Hakala, P. Törmä, *Physical Review B* **2017**, *95*, 15 155423.

[28] D. Khlopin, F. Laux, W. P. Wardley, J. Martin, G. A. Wurtz, J. Plain, N. Bonod, A. V. Zayats, W. Dickson, D. Gérard, *JOSA B* **2017**, *34*, 3 691.

[29] S. R. K. Rodriguez, A. Abass, B. Maes, O. T. Janssen, G. Vecchi, J. G. Rivas, *Physical Review X* **2011**, *1*, 2 021019.

Table of Contents

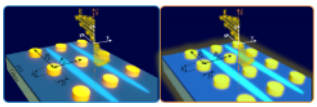

Low diffraction efficiency vs. high diffraction efficiency on the surface of rectangular arrays of gold nano-disks. The polarization set along x-direction enables the excitation of Rayleigh anomalies along the y-direction. The SLRs are strongly excited when the diffraction efficiency of the grazing orders is high, i.e. more energy is channeled onto the surface, which is obtained for small interparticle distances in the polarization direction.

[30] A. Abass, S. R.-K. Rodriguez, J. Gomez Rivas, B. Maes, *ACS Photonics* **2014**, *1*, 1 61.

[31] I. Abid, W. Safar, M. Edely, N. Felidj, M. Lamy de la Chapelle, H. Shen, *The Journal of Physical Chemistry C* **2022**, *126*, 20 8676.

[32] I. Allayarov, A. B. Evlyukhin, D. J. Roth, B. Chichkov, A. V. Zayats, A. Calà Lesina, *Advanced Photonics Research* **2024**, *5*, 1 2300268.

[33] G. W. Castellanos, P. Bai, J. Gómez Rivas, *Journal of Applied Physics* **2019**, *125*, 21 213105.

[34] V. E. Babicheva, A. B. Evlyukhin, *Journal of Applied Physics* **2021**, *129*, 4 040902.

[35] A. D. Utyushev, V. I. Zakomirnyi, A. E. Ershov, V. S. Gerasimov, S. V. Karpov, I. L. Rasskazov, *Photonics* **2020**, *7*, 2.

[36] A. D. Utyushev, V. I. Zakomirnyi, I. L. Rasskazov, *Reviews in Physics* **2021**, *6* 100051.

[37] V. E. Babicheva, A. B. Evlyukhin, *Laser & Photonics Reviews* **2017**, *11*, 6 1700132.

[38] J. van de Groep, A. Polman, *Opt. Express* **2013**, *21*, 22 26285.

[39] A. Ndao, R. Salut, M. Suarez, F. I. Baida, *Journal of Optics* **2018**, *20*, 4 045003.

[40] V. Tretnak, U. Hohenester, J. R. Krenn, A. Hohenau, *The Journal of Physical Chemistry C* **2020**, *124*, 3 2104.

[41] A. Hohenau, H. Ditlbacher, B. Lamprecht, J. R. Krenn, A. Leitner, F. R. Aussenegg, *Microelectronic Engineering* **2006**, *83*, 4-9 1464.

[42] J.-P. Berenger, *Journal of computational physics* **1996**, *127*, 2 363.

[43] M. Hamidi, F. I. Baida, A. Belkhir, O. Lamrous, *Journal of Physics D: Applied Physics* **2011**, *44*, 24 245101.